THE JOURNAL OF BIOLOGICAL CHEMISTRY VOL. 290, NO. 24, pp. 14826–14840, June 12, 2015

Genome Protection by the 9-1-1 Complex Subunit HUS1 Requires Clamp Formation, DNA Contacts, and ATR Signaling-independent Effector Functions*

Received for publication, December 6, 2014, and in revised form, April 15, 2015 Published, JBC Papers in Press, April 24, 2015, DOI 10.1074/jbc.M114.630640

Pei Xin Lim[‡], Darshil R. Patel[‡], Kelsey E. Poisson[‡], Manpreet Basuita[‡], Charlton Tsai[‡], Amy M. Lyndaker[‡], Bor-Jang Hwang[§], A-Lien Lu[§], and Robert S. Weiss[‡1]

From the [‡]Department of Biomedical Sciences, Cornell University, Ithaca, New York 14853 and the [§]Department of Biochemistry and Molecular Biology, University of Maryland School of Medicine, Baltimore, Maryland 21201

Background: The 9-1-1 complex mediates checkpoint signaling and repair.
Results: HUS1 functional residues for clamp formation, DNA contacts, and protein-protein association were identified.
Conclusion: HUS1 mediates checkpoint signaling-independent effector functions.
Significance: Learning how the 9-1-1 complex contributes to both checkpoint signaling and DNA repair is important for understanding the molecular mechanisms underlying a robust DNA damage response.

The RAD9A-HUS1-RAD1 (9-1-1) complex is a heterotrimeric clamp that promotes checkpoint signaling and repair at DNA damage sites. In this study, we elucidated HUS1 functional residues that drive clamp assembly, DNA interactions, and downstream effector functions. First, we mapped a HUS1-RAD9A interface residue that was critical for 9-1-1 assembly and DNA loading. Next, we identified multiple positively charged residues in the inner ring of HUS1 that were crucial for genotoxin-induced 9-1-1 chromatin localization and ATR signaling. Finally, we found two hydrophobic pockets on the HUS1 outer surface that were important for cell survival after DNA damage. Interestingly, these pockets were not required for 9-1-1 chromatin localization or ATR-mediated CHK1 activation but were necessary for interactions between HUS1 and its binding partner MYH, suggesting that they serve as interaction domains for the recruitment and coordination of downstream effectors at damage sites. Together, these results indicate that, once properly loaded onto damaged DNA, the 9-1-1 complex executes multiple, separable functions that promote genome maintenance.

When left unchecked, DNA insults from exogenous and endogenous sources can lead to premature aging, developmental defects, and tumorigenesis (1). To prevent these deleterious outcomes, cells have evolved DNA damage response (DDR)[2] pathways that are responsible for triggering an appropriate protective reaction to genome damage. Central to DDR pathways are checkpoint proteins that regulate cell cycle transitions, DNA repair, replication fork stability, and apoptosis (2).

The RAD9A-HUS1-RAD1 (9-1-1) clamp is a toroidal heterotrimeric DNA clamp that regulates checkpoint signaling after DNA damage (3). It is essential for cell survival after genotoxin exposure and during various physiological processes, such as embryogenesis, adult tissue homeostasis, and spermatogenesis (4–9). The 9-1-1 clamp is structurally related to proliferating cell nuclear antigen (PCNA), a homotrimeric processivity factor for DNA replication and repair (10). Like PCNA, each 9-1-1 subunit folds into two globular domains linked by an interdomain connecting loop (11–13). The subunits associate in a head-to-tail manner to form a stable heterotrimeric complex. A clamp loader composed of RFC1–5 loads PCNA at 3′ recessed DNA ends, whereas 9-1-1 is loaded by RAD17/RFC2–5 at 5′ recessed ends (14–16). Once loaded at damage sites, 9-1-1 stimulates ATR kinase activation through interactions with TOPBP1 (17). Activated ATR phosphorylates several substrates, including the effector kinase CHK1, which induce cell cycle arrest, stabilize stalled forks, and inhibit origin firing (2).

In addition to its checkpoint signaling functions, 9-1-1 also acts directly in DNA repair through its role as a molecular scaffold (3, 18, 19). The 9-1-1 clamp physically interacts with and stimulates the activity of factors in many DNA repair pathways, including base excision, mismatch, and nucleotide excision repair, as well as homologous recombination, non-homologous end joining, and translesion synthesis. Evaluating the physiological significance of these interactions is challenging because genetic approaches to ablate 9-1-1 function typically compromise both checkpoint signaling and all other functions executed by the clamp.

In order to resolve the relative importance of the checkpoint signaling-dependent and -independent functions of the 9-1-1 complex, we endeavored to identify residues that are essential for these functions and describe here residues in murine HUS1 (mHUS1) that mediate three critical 9-1-1 activities: clamp formation, DNA association, and interaction with downstream effectors. Consistent with the idea that 9-1-1 has critical signaling-independent roles, we identified HUS1 domains that

* This work was supported, in whole or in part, by National Institutes of Health Grants R01 CA108773 (to R. S. W.) and R01 CA78391 (to A. L.).
[1] To whom correspondence should be addressed: Dept. of Biomedical Sciences, Cornell University, Tower Rd., Ithaca, NY 14853-6401. Tel.: 607-253-4443; Fax: 607-253-4212; E-mail: rsw26@cornell.edu.
[2] The abbreviations used are: DDR, DNA damage response; 9-1-1, RAD9A-HUS1-RAD1; PCNA, proliferating cell nuclear antigen; mHUS1, murine HUS1; IF, immunofluorescence; IP, immunoprecipitation; PIP, PCNA-interacting protein; MMC, mitomycin C; MEF, mouse embryonic fibroblast; 4NQO, 4-nitroquinoline 1-oxide.

TABLE 1
Primers used for site-directed mutagenesis of *mHus1*

Mutations	Primer[a]
RAD9-interacting residue	
R128E	5′-gtctccatcgagcagcagcgaaatcgtggtgcatgatatc-3′
Inner ring hydrophobic cleft	
V19A,M22A,I23A	5′-cttgtctgaatcatttcacacgagccagtaacgcggcagccaagcttgccaaaacctgcac-3′
V247A	5′-gccggacagcaagcgactcccaccaag-3′
V271A,L273A	5′-atttgctcctggaagacgcctccgctcagtatttcatcccagc-3′
R18A	5′-ctatcatgttactgactgctgtgaaatgattcagacaagccagg-3′[b]
R18Q	5′-cttgtctgaatcatttcacacaagtcagtaacatgatagccaa-3′
R18Q,M22T	5′-cttgtctgaatcatttcacacaagtcagtaacacgatagccaagcttgcca-3′
Inner ring positively charged residues	
R18A	5′-ctatcatgttactgactgctgtgaaatgattcagacaagccagg-3′[b]
K25A	5′-ggtgcaggttttggcaagcgcggctatcatgttactgact-3′[b]
K25A,K28A	5′-atgcggagggtgcaggttgcggcaagcgcggctatcatgttactgac-3′[b]
K93A	5′-tctggagttctgggcagttgccaaggctcgagataagttt-3′[b]
R90A,K93A	5′-tggagttctgggcagttgccaaggctgcagataagttttccgacgttaattctaa-3′[b]
K165A	5′-ccacaacactcttcatcatcgccaaggctggtaagcaaatac-3′[b]
K165A,K168A	5′-gtttctcatttttttccacaacactcgccatcatcgccaaggctggtaagcaaatactgacg-3′[b]
K173A,R175A	5′-ttcaatcacaagctgattgctgatgtttgccattgcttccacaacactcttcatcatcttcaag-3′[b]
K236A,K237A	5′-aagaaactggaggagtgccgctatgtcaatgtgcaccttggccatgtcttct-3′[b]
Outer ring hydrophobic pocket	
P150A	5′-gtggaaggacttacaagaagcctccatcccagac-3′
P150A,I152A,P153A,C155A	5′-gactgtggaaggacttacaagaagcctccgccgcagacgctgacgtcagtatttgcttt-3′
V257A,T261A	5′-caaggcagtgtgcaatattgcgaataacagagctgttcattttgatttgctc-3′
F276A,P278A	5′-aagacgtctcccttcagtatgccatcgcagccttgtcctagg-3′
S53R	5′-gctcacaccacatcctcacgcctccac-3′[b]
I152R	5′-gacttacaagaaccctccagaccagactgtgacgtcag-3′
I152Y	5′-aaggacttacaagaaccctcctacccagactgtgacgtcagtatt-3′
I152F	5′-cttacaagaaccctcctttcccagactgtgacgt-3′
Outer ring novel pocket	
F3A	5′-[ccgcgtggatcc]atgaaggctcgcgccaagatcg-3′[c]
F3R	5′-cgcgtggatccatgaagcgtcgcgccaagatcgtggacc-3′
F3R,R4A	5′-cgcgtggatccatgaaggctgccgccaagatcgtggacct-3′
G71W	5′-gaacttttttagtgaatttcaaatggaatgggtctctgaagaaaacaacgagattt-3′
I79A	5′-aggagtctctgaagaaaacaacgaggcttatttagaattaacgtcggaaaac-3′
L105A	5′-ccagagccttgaaaatcaaggcgactaacaaacactttccct-3′
K104A,L105A,T106A	5′-ccagaactccagagccttgaaaatcgcggcggctaacaaacactttccctgtcttac-3′
V138A,L139D	5′-gcatgatatccccataaaggctgatccgagaagactgtggaagg-3′
L105R	5′tccagagccttgaaaatcaagaggactaacaaacactttccctg-3′
L139R	5′-tcgtggtgcatgatatccccataaaggttagaccgagaagactgtgg-3′
R4D	5′-[cgcgtggatcc]atgaagtttgacgccaagatcgtggacc-3′[c]
F3R,R4D	5′-[cgcgtggatcc]atgaagcgtgacgccaagatcgtggacc-3′[c]
Outer ring positively charged residues	
K2A,R4A,K6A	5′-gacaagccaggtccacgatcgcggcggcaaacgccat[gaatccacgcgg]-3′[b,c]
R99A,K102A,K104A	5′-gggaaagtgtttgttagtcagcgcgattgccaaggctgcggagttctgggcagttttcaagg-3′[b]
K108A,H109A	5′-cagacacggtaagacagggaaaggctgcgttagtcagcttgattttcaagg-3′[b]
K137A,R141A,R142A,K145A	5′-ggttcttgtaagtccgcccacagtgctgccggaagaaccgctatggggatatcatgcaccacgattc-3′[b]
BII4-6 loop	
Δ215–227	5′-gtgcaccttggccat ()taatagagggttttcaagatccttaaaa-3′[b,d]
Δ215–227::hHus1 loop	5′-attttaaggatcttgaaaaccctctattagcctctgaaagtacccatgaaaacagacacccagaagacatggcca-3′ 5′-gcctctgaaagtacccatgaagacagaaacgtagaacacatggccaaggtgcaca-3′
Δ215–227::PCNA loop	5′-cattttaaggatcttgaaaaccctctattacaaactagcaatgtcgatcaaaacagacacccagaagacatggccaag-3′ 5′-cttgaaaaccctctattacaaactagcaatgtcgataaagaagaagaggcagtagacatggccaaggtgcacat-3′

[a] The positions of nucleotides altered to create desired mutations are underlined.
[b] Antisense primers. Primer orientation was chosen based on lower energy cost of mismatches.
[c] pGEX-2T sequences shown in brackets.
[d] (), 39 nucleotides deleted.

are dispensable for ATR-mediated signaling to CHK1 but nevertheless required for the cellular response to DNA damage.

Experimental Procedures

Plasmids and Mutagenesis—All mutations were introduced into *mHus1* using a QuikChange Lightning multisite-directed mutagenesis kit (Agilent Technologies) and the primers listed in Table 1. Most mutagenesis was performed on the pBP2-mHus1 retroviral plasmid (20) as the template with two exceptions. In the first case, where compound mutations had to be made sequentially, pBP2-mHus1 plasmids with intermediate mutations were used as the template. In the second case, residues Lys-2, Phe-3, Arg-4, and Lys-6 of mHUS1 were mutagenized with the pGEX2T-mHus1 plasmid as the template because 5′ retroviral long terminal repeats in the pBP2-mHus1 plasmid interfered with mutagenesis. Subsequently, the pGEX2T-mHus1 mutants were subcloned into pBP2 plasmid. Functionally defective mutant constructs were further subcloned into pCMV-neo-Bam$_3$ plasmid (21) for mutant mHUS1 immunoblot detection as well as into p3XFLAG-CMV^{TM}-14 (Sigma) for immunofluorescence (IF) and chromatin fractionation assays. All mutations were verified by DNA sequencing.

Cell Culture, Retroviral Infection and Transfection—All cultured cells were grown on gelatinized dishes in Dulbecco's modified Eagle's medium (Corning Inc.) supplemented with 10% bovine calf serum (Thermo Scientific Hyclone, SH30072),

TABLE 2
List of UniProtKB accession numbers of the PCNA, RAD9A, HUS1, and RAD1 sequences used for evolutionary conservation analysis

Organism	Symbol	Accession numbers			
		PCNA	RAD9A	HUS1	RAD1
Ailuropoda melanoleuca (giant panda)	AILME	D2HQS7	G1L1M9	G1LDT0	G1L9B8
Arabidopsis thaliana (mouse-ear cress)	ARATH	Q9M7Q7	F4J7B7	Q709F6	Q8L7G8
Bos taurus (bovine)	BOVIN	Q3ZBW4	Q5EAC3	E1BG06	E1BB72
Caenorhabditis elegans (nematode worm)	CAEEL	O02115	Q9NBJ6	G5EFI9	G5EC44
Callithrix jacchus (white-tufted-ear marmoset)	CALJA	F7GZC8	U3DMA2	F7G3C8	F7I3N9
Canis familiaris (dog)	CANFA	E2R0D6	F6XPS6	F1Q245	E2QYH8
Cavia porcellus (guinea pig)	CAVPO	H0VE65	H0VIK1	H0WC14	H0VEA3
Ceratitis capitata (Mediterranean fruit fly)	CERCA	W8B157	W8C9F2	W8C4C2	W8B5C0
Gallus gallus (chicken)	CHICK	Q9DEA3	R4GG06	E1C8I4	E1C4I3
Chlamydomonas reinhardtii (*Chlamydomonas smithii*)	CHLRE	A8JHX0	A8IS48	A8J5N4	A8IFX0
Dictyostelium discoideum (slime mold)	DICDI	Q54K47	Q869Q1	Q54NC0	Q55E62
Drosophila melanogaster (fruit fly)	DROME	P17917	O96533	Q9VN60	Q9VQD4
Felis catus (cat)	FELCA	M3WAR4	M3W096	M3XC14	M3WY16
Equus caballus (horse)	HORSE	F6R950	F6QXP4	F7BM24	F6YZW4
Homo sapiens (human)	HUMAN	P12004	Q99638	O60921	O60671
Hydra vulgaris (hydra)	HYDVU	T2MHJ2	T2M799	T2MIV2	T2MID6
Lepisosteus oculatus (spotted gar)	LEPOC	W5NF42	W5MKE2	W5N6Y6	W5N1G5
Loxodonta africana (African elephant)	LOXAF	G3SY50	G3T2S3	G3TJN6	G3SZN1
Macaca mulatta (rhesus macaque)	MACMU	F6ZD63	H9FXY2	F7F1Y2	F7A5K9
Mus musculus (mouse)	MOUSE	P17918	Q9Z0F6	Q8BQY8	Q9QWZ1
Mustela putorius furo (European domestic ferret)	MUSPF	M3Y491	M3XXF9	M3Z395	M3YUM0
Myotis lucifugus (little brown bat)	MYOLU	G1NW67	G1P3Z2	G1NTI5	G1PS54
Neovison vison (American mink)	NEOVI	U6DX35	U6D1D1	U6CPZ2	U6CY10
Nomascus leucogenys (northern white-cheeked gibbon)	NOMLE	G1R863	G1R3F3	G1QWZ3	G1RWE2
Oreochromis niloticus (Nile tilapia)	ORENI	I3KAK2	I3JC68	I3K6T5	I3JLK1
Ornithorhynchus anatinus (duckbill platypus)	ORNAN	F7BRC7	F6REC2	F7BS27	F6UI60
Otolemur garnettii (small-eared galago)	OTOGA	H0XLL4	H0XWZ7	H0X7H9	H0XC10
Pan troglodytes (chimpanzee)	PANTR	H2QJX3	K7DL38	H2QUJ9	K7BUE0
Sus scrofa (pig)	PIG	I3L813	F1RUX7	B6UV60	F1SND5
Polysphondylium pallidum (cellular slime mold)	POLPA	D3BSY5	D3BA05	D3BR17	D3BPJ7
Pongo abelii (Sumatran orangutan)	PONAB	H2P1A0	H2NCN7	H2PXG5	Q5R7X9
Oryctolagus cuniculus (rabbit)	RABIT	G1SKZ3	G1TKX6	G1TRN1	G1T7G8
Rattus norvegicus (rat)	RAT	P04961	D3ZXM2	D3ZNA8	D3ZC52
Sarcophilus harrisii (Tasmanian devil)	SARHA	G3WDY3	G3VT27	G3W0W1	G3WBB6
Schizosaccharomyces pombe (fission yeast)	SCHPO	Q03392	P26306	P78955	P22193
Ovis aries (sheep)	SHEEP	W5Q6P4	W5PNJ1	W5PS82	W5PPP9
Spermophilus tridecemlineatus (thirteen-lined ground squirrel)	SPETR	I3NDE1	I3NF38	I3MYM9	I3MDU2
Strongylocentrotus purpuratus (purple sea urchin)	STRPU	W4Z5C9	W4YCU0	W4ZAK8	W4ZIN8
Tetraodon nigroviridis (spotted green pufferfish)	TETNG	H3DD39	H3D6H6	H3D7M2	H3BWC7
Wickerhamomyces ciferrii (yeast)	WICCF	K0KS34	K0KG77	K0KFL9	K0KTE1
Xenopus laevis (African clawed frog)	XENLA	P18248	Q7ZZU5	Q8JHD8	Q8AY27
Xenopus tropicalis (Western clawed frog)	XENTR	Q66KJ8	Q6DJ26	Q6DF51	A9ULD8
Xiphophorus maculatus (Southern platyfish)	XIPMA	M4AKD0	M4A625	M4AET7	M3ZPZ4
Saccharomyces cerevisiae (bakers' yeast)	YEAST	P15873	Q08949	Q02574	P48581

1% nonessential amino acids (Corning Cellgro, 25-025-CI), 1% L-glutamate (25-005-CI), and 1% penicillin and streptomycin (30-002-CI). Expression of the various *mHus1* constructs in *Hus1*$^{-/-}$*p21*$^{-/-}$ mouse embryonic fibroblasts (MEFs) and HEK293T cells (ATCC) was done in two ways. The first method was pBabe-based retroviral transduction for low level ectopic *Hus1* expression as described previously (20). The second method was plasmid transfection of pCMV-mHus1 and pCMV-mHus1–3XFLAG high level expression constructs done as follows. A mix of 575 μl of DMEM, 40 μg of polyethyleneimine, 4 μg of pCMV plasmid, and 1 μg of pGK-puro plasmid was dripped onto 10^6 *Hus1*$^{-/-}$ *p21*$^{-/-}$ MEFs seeded the day before in a 10-cm dish. Transfected cells were selected in culture medium containing 1.83 μg/ml puromycin, replaced every other day for a week. Stable drug-resistant cells made from both methods were cultured according to the 3T3 passaging protocol for maintenance and experimental use. For co-immunoprecipitation (co-IP) assays, pCMV-mHUS1 constructs were co-transfected with pCMV-hRad9a-Myc and pCMV-hRad1-HA plasmids.

Survival Assays—For short term viability assays, cells were seeded in 6-well plates and either left untreated or treated with 50 ng/ml 4NQO or 0.5 μM aphidicolin for 24 h. Mitomycin C (MMC) treatment was for 1 h. After 3 days, the cells were collected by trypsinization and counted using a Moxi^{TM} Z mini automated cell counter (ORFLO Technologies). Percentage survival was calculated by dividing the number of cells after treatment by the number of untreated cells. *Error bars* in the figures show S.D. Statistical analysis was by Student's *t* test, and *p* values of <0.05 were considered significant. For clonogenic survival assays, cells were seeded in 6-well plates and treated with 4NQO or aphidicolin for 24 h or with MMC for 1 h. After 6 days, the cells were fixed with methanol and stained with crystal violet overnight. The plates were then washed, dried, and scanned.

ConSurf Evolutionary Conservation and Surface Electrostatic Potential Analyses—Amino acid sequences of PCNA, RAD9A, HUS1, and RAD1 from 44 organisms that represent a broad range of taxa were curated from the UniProtKB database (Table 2). Multiple sequence alignments were created with ClustalX version 2.1 (22) and uploaded to the ConSurf server (23) for calculation of evolutionary conservation scores (Bayesian method) with reference to the human counterparts of each protein. The scores were projected on available protein structures

of PCNA (Protein Data Bank code 1VYM) and RAD9A-HUS1-RAD1 (Protein Data Bank code 3GGR) to identify functional surface residues. All images were created using PyMOL. The surface electrostatic potential of HUS1 was calculated and displayed using the Adaptive Poisson-Boltzmann Solver plugin in PyMOL. In the calculations, dielectric constants of 1.0 and solvent ionic strength equivalent to 75 mM KCl were used. Side chains of lysine and arginine residues were assigned a net positive charge, aspartate and glutamate were assigned a negative charge, and other residues were neutral. Positive and negative color contours were set at $\pm 10kT/e$.

Immunoprecipitation and Immunoblotting—For analysis of 9-1-1 subunit interactions, HEK293T cells transiently transfected with pCMV-mHus1, pCMV-hRad9a-Myc, and pCMV-hRad1-HA constructs were irradiated with 100 J/m^2 UV, and 2 h later, cell lysates for co-IP were prepared. Lysates were incubated with anti-MYC (Santa Cruz Biotechnology, Inc.) or anti-HA (Covance) antibodies, followed by incubation with protein A/G resin (Thermo Scientific). For analysis of HUS1-MYH interactions, HEK293T transiently transfected with pCMV-mHus1–3XFLAG or pCMV-R4D,I152Y-3XFLAG constructs were treated with 1 mM H_2O_2, and 3 h later, cell lysates for co-IP were prepared. Lysates were incubated with anti-FLAG resin (Sigma). Immunoprecipitates or total cell lysates (input) were resolved by SDS-PAGE. Standard immunoblotting procedures were performed using antibodies specific for HUS1 (8), RAD9A (8), MYC (Santa Cruz Biotechnology), HA (Covance), FLAG (Sigma), pCHK1 Ser-345 (Cell Signaling), histone 3 (Abcam), GAPDH (Advanced ImmunoChemical), MYH (24), TOPBP1 (25), or β-actin (Sigma).

Immunofluorescence—Hus1$^{-/-}$*p21*$^{-/-}$ MEFs stably expressing WT or mutant mHUS1–3XFLAG proteins were grown on gelatinized coverslips overnight and treated with MMC for 23 h. Cells were immunostained with mouse α-FLAG and rabbit α-RAD9A primary antibodies and Alexa Fluor 488 goat α-mouse and Alexa Fluor 555 goat α-rabbit secondary antibodies (Life Technologies, Inc.) for IF detection according to the antibody manufacturer's protocol. Overlapping FLAG and RAD9A foci in 50 randomly picked cells from each sample were quantified and analyzed by one-way analysis of variance. p values of <0.05 were considered significant.

Chromatin Fractionation—Hus1$^{-/-}$*p21*$^{-/-}$ MEFs stably expressing WT or mutant mHUS1–3XFLAG proteins were irradiated with 100 J/m^2 UVC and fractionated 2 h post-treatment using a previously described extraction protocol (26) with modifications. Cells were swollen in hypotonic buffer (10 mM HEPES, pH 7.9, 1.5 mM $MgCl_2$, 75 mM KCl, 0.2 mM PMSF, and 0.5 M DTT) for 6 min in 37 °C and lysed with a Dounce homogenizer. After centrifugation at 14,000 rpm for 15 min, the supernatant was separated for cytoplasmic extract preparation. The nuclei pellet was resuspended in equal volumes of low salt and high salt buffers (20 mM HEPES, pH 7.9, 25% glycerol, 1.5 mM $MgCl_2$, 0.2 or 1.2 M KCl, 0.2 mM EDTA, 0.2 mM PMSF, and 0.5 M DTT) in sequential order to extract the soluble nuclear fraction. After centrifugation at 14,000 rpm for 30 min, the supernatant was separated for nuclear extract preparation. The pellet was resuspended in radioimmune precipitation assay buffer (50 mM Tris, pH 8.0, 150 mM NaCl, 5 mM EDTA, 50 mM NaF, 0.5% deoxycholate, 1% Nonidet P-40, and 0.1% SDS) supplemented with aprotinin, leupeptin, sodium orthovanadate, and phenylmethylsulfonyl fluoride (PMSF), sonicated at 24–30 watts for 1 min (Misonix Sonicator 3000), and centrifuged to produce the chromatin fraction in the supernatant. The cytoplasmic and nuclear fractions were dialyzed in dialysis buffer (20 mM HEPES, pH 7.9, 20% glycerol, 100 mM KCl, 0.2 mM EDTA, 0.2 mM PMSF, and 0.5 M DTT) overnight before use. 20 μg of each fraction was used for immunoblotting.

Results

A Systematic Structure/Function Analysis of HUS1—We used published crystal structure analyses of human 9-1-1 (11–13), computational modeling of 9-1-1 subunit and DNA interactions (27, 28), and evolutionary conservation analysis to predict functionally important mHUS1 residues. Initially we screened mHUS1 mutants with targeted mutations in seven specific regions (Table 3) for the ability to complement the genotoxin sensitivity of *Hus1*$^{-/-}$*p21*$^{-/-}$ MEFs, which are hypersensitive to DNA damage (6). As detailed below, three HUS1 regions (the HUS1/RAD9A interface, the positively charged inner surface of HUS1, and two hydrophobic pockets on the HUS1 outer surface) emerged as having the greatest functional significance in complemented cells challenged with 4NQO, a UV mimetic, or aphidicolin, a replication stress-inducing DNA polymerase inhibitor.

HUS1-RAD9A Interaction Is Critical for 9-1-1 Clamp Formation and Function—Stable intersubunit interactions are required to allow 9-1-1 clamp formation and maintain clamp integrity during the loading process (11–13). We tested the impact of disrupting intersubunit interactions by targeting mHUS1 Arg-128 (Arg-127 in hHUS1) located at the HUS1-RAD9A interface (Fig. 1*A*), because its polar interactions were predicted to contribute substantially to the interaction between these subunits (28). Indeed, mutation of the orthologous residue in *Schizosaccharomyces pombe hus1* (Asn-121) impairs association with spRAD9A (29). Hence, we mutated Arg-128 to Glu (R128E) to reverse the charge of the residue and analyzed 9-1-1 clamp formation and cell survival after genotoxin treatment. After confirming the stability of R128E mutant protein (Fig. 1*B*), we subjected R128E-expressing *Hus1*-null MEFs to short term viability and clonogenic survival assays (Fig. 1, *C* and *D*). In both assays, mHUS1 R128E failed to rescue the genotoxin hypersensitivity of *Hus1*-null MEFs. Next, co-IP assays were performed to test interactions between mHUS1 R128E and RAD9A (Fig. 1*E*). Whereas wild-type (WT) mHUS1 co-immunoprecipitated with hRAD9A-MYC, mHUS1 R128E did not. Interestingly, in R128E-expressing cells, hRAD1-HA also was not detected in the MYC immunoprecipitate, and neither mHUS1 R128E nor hRAD9A-MYC was detected in the reciprocal HA immunoprecipitate (Fig. 1*E*). These results indicate that reversing the charge of a single residue at the HUS1-RAD9A interface fully disrupted the stability and function of the entire trimeric 9-1-1 complex.

Multiple Positively Charged Residues on the HUS1 Inner Surface Facilitate HUS1-DNA Interactions in a Synergistic Manner—Like PCNA, 9-1-1 is thought to interact with the DNA phosphate backbone, affording proper loading and scaf-

TABLE 3
Summary of clonogenic survival and short term viability assay results for all mHUS1 mutants analyzed

Mutations	Expression	Clonogenic survival[a]		Short term viability[a]	
		4NQO	Aphidicolin	4NQO	Aphidicolin
RAD9-interacting residue					
R128E	Yes	Null	Null	Null	Null
Inner ring hydrophobic cleft					
V19A,M22A,I23A	Partial	WT	WT	WT	WT
V247A,V271A,L273A	Partial	WT	WT	WT	WT
V19A,M22A,I23A,V247A,V271A,L273A	Partial	WT	Partial	Partial	Null
R18A	Yes	NT[b]	NT	WT	WT
R18Q	Yes	NT	NT	WT	WT
R18Q,M22T	Yes	NT	NT	WT	WT
Inner ring positively charged residues					
K93A	NT	WT	WT	WT	WT
K25A	NT	WT	WT	WT	WT
K25A,K93A	Yes	WT	WT	WT	WT
K25A,K236A,K237A (3A)	Yes	Partial	Partial	Partial	WT
K173A,R175A,K236A,K237A (4A-1)	Yes	WT	Partial	Partial	Partial
K25A,K93A,K236A,K237A (4A-2)	Yes	Null	Null	Null	Null
K25A,K93A,K173A,R175A,K236A,K237A (6A)	Yes	Null	Null	Null	Null
R90A,K93A (C1)	Yes	WT	WT	WT	Partial
R18A,K25A,K28A (C2)	NT	WT	WT	WT	WT
K236A,K237A (C3)	NT	WT	WT	WT+	WT
K165A,K168A,K173A,R175A (C4)	Yes	WT	Partial	WT	Partial
R18A,K93A,K165A (C5)	Yes	WT	Partial	Partial	WT
K173A,R175A	NT	WT	WT	WT+	WT
K165A,K168A	NT	WT	WT	NT	NT
K25A,K28A,K165A	Not stable	NT	NT	NT	NT
Outer ring hydrophobic pocket					
P150A,I152A,P153A,C155A	Partial	WT	WT	Partial	Partial
V257A,T261A,F276A,P278A	Yes	WT	WT	WT	WT
P150A,I152A,P153A,C155A,V257A,T261A,F276A,P278A	Partial	WT	Partial	NT	NT
P150A,V257A,T261A,F276A,P278A	Partial	WT	Partial	WT	Partial
P150A,I152A,P153A,C155A,F276A,P278A	Not stable	Partial	Partial	Partial	Partial
S53R	Yes	NT	NT	WT	WT
I152R	Partial	NT	NT	Partial	Partial
I152Y	Yes	Partial	WT	Partial	Partial
I152F	Yes	NT	NT	WT	WT
Outer ring novel pocket					
F3A,G71W,I79A,L105A	Not stable	Null	Null	NT	NT
F3A,G71W	NT	WT	WT	NT	NT
F3A,I79A	NT	WT	WT	NT	NT
F3A,L105A	NT	WT	WT	NT	NT
F3A,I79A,L105A	Not stable	WT	Null	NT	NT
F3R	Not stable	Partial	Partial	Partial	WT
F3R,R4A	NT	Partial	Partial	Partial	WT
K104A,L105A,T106A	NT	WT	WT	WT	Partial
K104A,L105A,T106A,V138A,L139D	Not stable	Null	Null	Null	Null
L105R	Not stable	NT	NT	NT	NT
L139R	Not stable	NT	NT	NT	NT
R4D	Yes	Partial	WT	Partial	Partial
R4D,I152Y	Yes	Partial	WT	Partial	Partial
Outer ring positively charged residues					
K2A,R4A,K6A	NT	WT	WT	NT	NT
R99A,K102A,K104A	NT	WT	WT	NT	NT
K108A,H109A	NT	WT	WT	NT	NT
K137A,R141A,R142A,K145A	NT	WT	WT	NT	NT
BII4-6 loop					
Δ215–227	Not stable	Null	Null	NT	NT
Δ215–227::hHus1 loop	NT	WT	WT	NT	NT
Δ215–227::PCNA loop	NT	WT	WT	NT	NT

[a] Survival outcomes were categorized as follows: WT+ (better than WT mHUS1-complemented cells), WT (similar to WT mHUS1-complemented cells), Partial (worse than WT mHUS1 complemented cells but better than *Hus1*-null cells), and Null (similar to *Hus1* null cells).
[b] NT, not tested.

folding activity on chromatin (30). The inner HUS1 surface consists of four parallel α-helices containing 11 positively charged residues (Fig. 2*A*). In order to determine the importance of mHUS1-DNA contacts, alanine mutants of several of these residues (Lys-25, Lys-93, Lys-173, Arg-175, Lys-236, and Lys-237) were generated and functionally tested. These mutations did not disrupt mHUS1 protein stability (Fig. 2*B*), but all caused loss of function as evidenced by partial (mutants 3A and 4A-1) or complete (4A-2 and 6A) genotoxin hypersensitivity phenotypes (Fig. 2, *C* and *D*). These defects were not due to disruption of 9-1-1 clamp formation, because both mHUS1 4A-2 and 6A co-immunoprecipitated with hRAD9A-MYC and hRAD1-HA to the same extent as WT mHUS1 (Fig. 2*E*). Notably, the hHUS1 residues equivalent to those mutated in 4A-2 and 6A were computationally predicted to directly contact DNA (27). We generated additional mutants in different alignments (Fig. 3*A* and Table 3) to investigate the possible involvement of alternative DNA contacts. However, these mutants

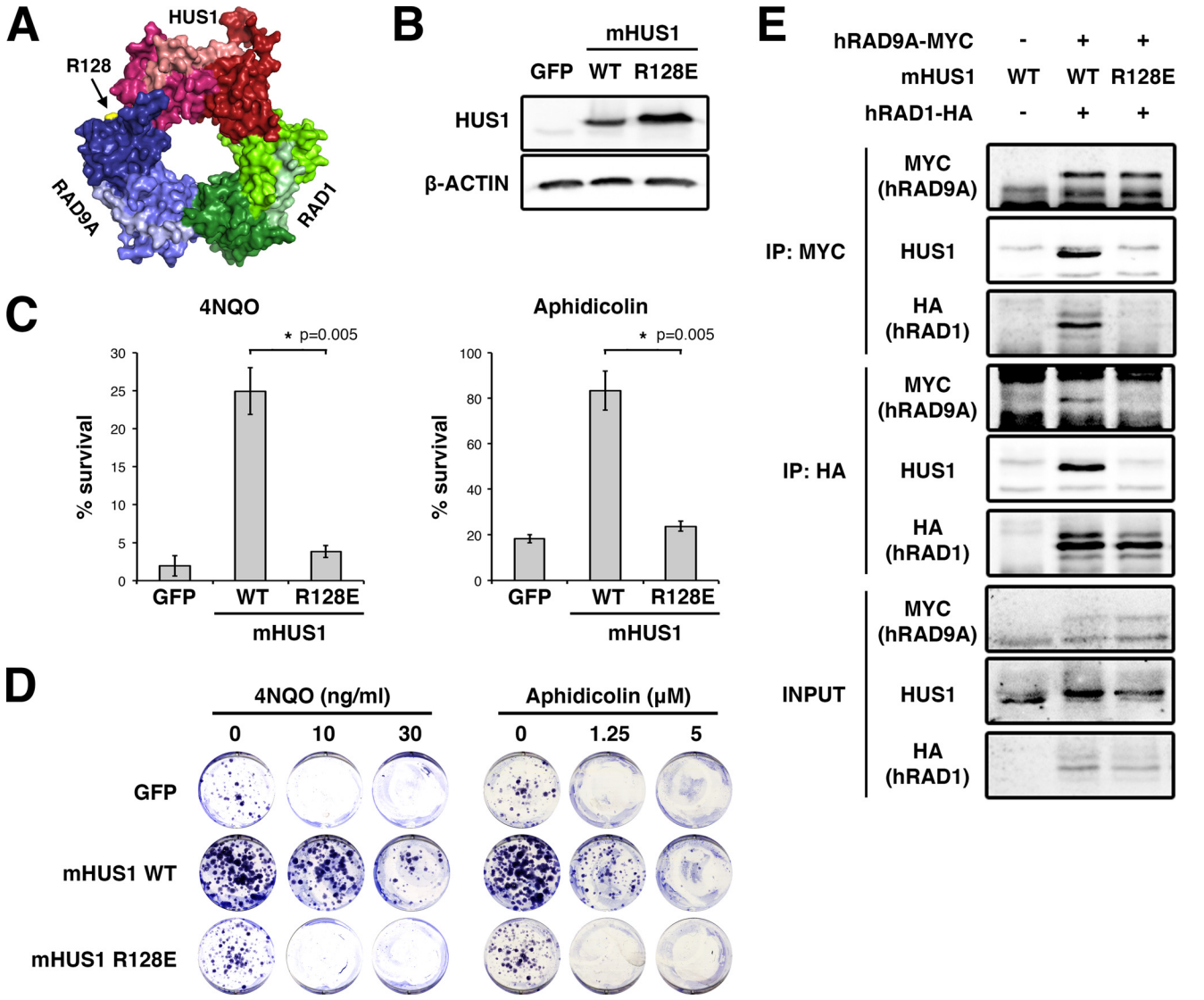

FIGURE 1. **mHUS1 residue Arg-128 is crucial for 9-1-1 clamp formation.** *A*, Arg-128 (*arrow*) is located at the HUS1-RAD9A interface (Protein Data Bank code 3GGR). *B*, immunoblotting using antibodies specific for HUS1 or β-actin was performed to compare the stability of WT and R128E mHUS1 proteins in HEK293T cells. *C* and *D*, short term viability and clonogenic survival were measured for *Hus1*-null MEFs stably expressing mHUS1 R128E after 4NQO or aphidicolin treatments. MEFs expressing GFP or WT mHUS1 served as negative and positive controls, respectively. Each experiment in *C* was repeated five times with two independently generated cell lines. *E*, interaction of mHUS1 R128E with hRAD9 and hRAD1 was assessed by co-IP. *Error bars*, S.D.

were not associated with pronounced hypersensitivity phenotypes (Fig. 3*B*). Taken together, these results indicate that 6 specific positively charged HUS1 residues synergistically facilitate HUS1-DNA contacts and are necessary for cell survival following DNA damage.

HUS1 Has Two Functional Hydrophobic Pockets That Are Important for Genome Maintenance—Like PCNA, the 9-1-1 clamp stimulates the activity of many DNA repair factors via direct physical interactions. To identify HUS1 functional domains that might bind effectors, we conducted an evolutionary conservation analysis with the assumption that functional residues would be evolutionarily conserved. As a proof of principle, we first performed this analysis on PCNA (Fig. 4*A*). Two clusters of conserved residues were apparent on the PCNA outer ring surface, one for the well characterized primary PCNA-interacting protein (PIP) box binding pocket and the other for a secondary domain that also associates with sequences C-terminal to the PIP box motif in some PCNA effectors (31, 32).

The same analysis was then applied to RAD9A, HUS1, and RAD1 (Fig. 4*A*). Structural studies had previously identified PCNA-like hydrophobic pockets in RAD9A and HUS1 (12). However, the distribution of conserved residues for each subunit varied from PCNA and from each other. RAD9A showed conservation of the primary PCNA-like hydrophobic pocket, but HUS1 and RAD1 did not. However, when analyzing only mammalian sequences, conservation of HUS1 and RAD1 residues at the equivalent position for the primary PCNA-like hydrophobic pocket became evident (data not shown). We also identified a cluster of conserved HUS1 residues in the topologically equivalent region of the PCNA secondary binding site. This pocket is formed by 3 hydrophobic HUS1 residues (Phe-3, Ile-79, and Leu-105)

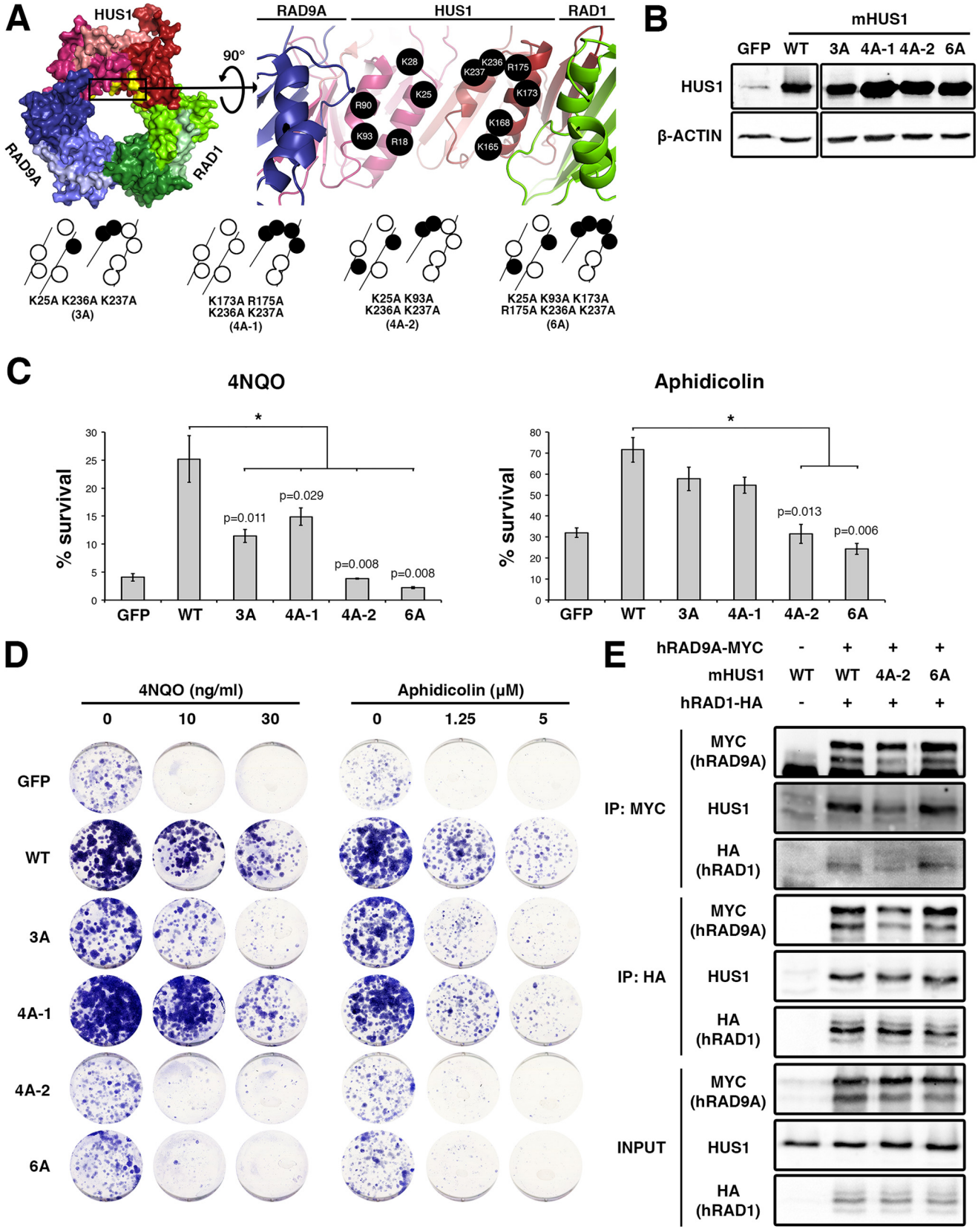

FIGURE 2. **Multiple positively charged residues on the HUS1 inner ring are synergistically important for genotoxic stress responses.** *A*, mHUS1 has 11 arginines and lysines (*black circles*) distributed on four α-helices in the inner ring surface (Protein Data Bank code 3GGR). Alanine substitutions of these residues (*3A-6A*) were made. *B*, protein expression was measured as in Fig. 1*B*. *C* and *D*, genotoxin sensitivity was measured as in Fig. 1, *C* and *D*. Each experiment in *C* was repeated three times with three independently generated cell lines. *E*, interaction of mHUS1 mutant proteins with hRAD9 and hRAD1 was assessed by co-IP. *Error bars*, S.D.

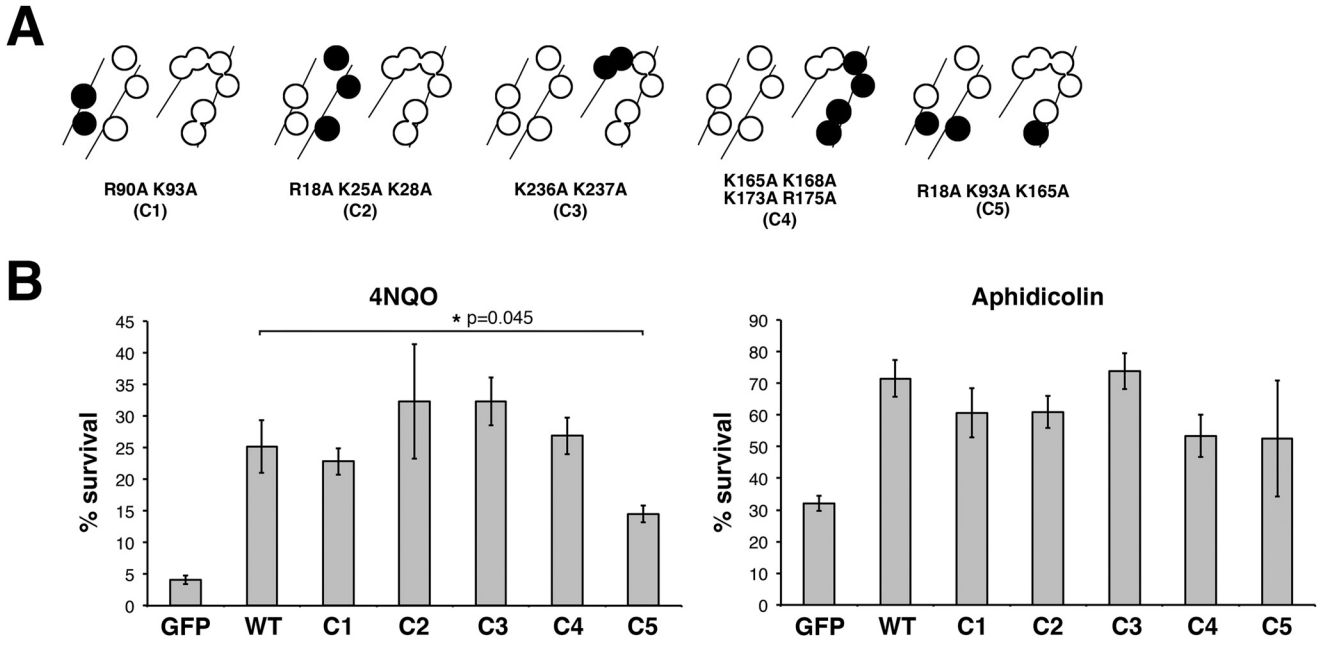

FIGURE 3. **Certain configurations of positively charged residues in the inner ring of HUS1 are dispensable for genotoxic stress responses.** *A*, alanine substitutions of positively charged residues were made in various combinations (*C1–C5*), as indicated by the *filled circles*. *B*, short term viability of *Hus1*$^{-/-}$ *p21*$^{-/-}$ MEFs stably expressing mHUS1 inner ring mutants C1–C5 after 4NQO or aphidicolin treatments was measured. Each experiment was repeated four times using three independently generated cell lines. No significant differences in survival between wild-type mHUS1 and mutants C1–C5 were identified, except for C5 with 4NQO treatment. *Error bars*, S.D.

along with Arg-4 at the pocket base, creating a strong positive electrostatic potential surrounded by a neutral field (Fig. 4, *B* and *C*).

To assess the functional significance of the HUS1 outer surface domains, we first targeted hydrophobic residues that form the PCNA-like primary and secondary pockets, but various alanine mutants either disrupted HUS1 protein stability or did not cause loss of function in survival assays (Table 3). We then generated mutations predicted to physically or electrostatically block the pockets (Fig. 5*A*). For the primary pocket, we changed Ile-152 (Val-151 in hHUS1) to Tyr (I152Y) to block the pocket with a bulky side chain. For the secondary pocket, Arg-4 was mutated to D (R4D) to reverse the charge at the base. We also generated the double pocket mutant (R4D,I152Y) to test whether the pockets functioned independently or in conjunction with each other. Although all three mutants were stably expressed and competent for clamp formation (Fig. 5, *B* and *E*), *Hus1*-deficient cells expressing the double pocket mutant were no more sensitive to 4NQO or aphidicolin than those expressing either single pocket mutant (Fig. 5, *C* and *D*). Interestingly, when challenged with MMC, cells expressing the double pocket mutant showed a synergistic increase in hypersensitivity as compared with the single mutants. These results suggest that the two HUS1 outer surface pockets have separable roles in response to certain forms of DNA damage, such as DNA cross-links, but act in conjunction for other DNA lesions, such as those induced by 4NQO or aphidicolin.

DNA Damage-induced HUS1 Chromatin Localization Is Disrupted in Clamp-destabilizing and DNA Interaction Mutants but Occurs Normally in Pocket Mutants—In order to determine how the different classes of HUS1 mutations affected the ability of HUS1 to localize on chromatin after DNA damage, we performed IF assays in *Hus1*-null MEFs complemented with 3XFLAG-tagged mHUS1 mutants, including R128E (RAD9A interface), 4A-2 or 6A (DNA binding), or I152Y or R4D (outer surface pockets) (Fig. 6*A*). We quantified RAD9A and FLAG IF co-staining in cells treated with MMC (Fig. 6*C*). MMC-induced RAD9A foci were absent in *Hus1*-null MEFs but were present after restoration of mHUS1 expression. Whereas RAD9A and FLAG foci colocalized in MEFs expressing WT mHUS1–3XFLAG, probably representing 9-1-1 accumulation on damaged DNA, the clamp-destabilizing HUS1 mutant R128E-3XFLAG failed to form FLAG or RAD9A foci. Similar results were observed for 4A2–3XFLAG and 6A-3XFLAG DNA interaction mutants. By comparison, inner ring mutants with less severe genotoxin sensitivity phenotypes showed an intermediate average number of MMC-induced foci formation (Fig. 6, *B* and *D*), suggesting that 9-1-1 loading requires clamp-DNA interactions, as is the case for PCNA (30). By contrast, mHUS1 pocket mutants I152Y-3XFLAG, R4D-3XFLAG, and R4D, I152Y-3XFLAG retained the ability to form MMC-induced foci and colocalize with RAD9A to the same extent as WT mHUS1–3XFLAG (Fig. 6, *A* and *C*).

To verify the IF results, we performed immunoblotting of fractionated cells after UV irradiation (Fig. 6*E*). WT mHUS1-3XFLAG was detected in the nuclear and chromatin compartments after UV damage. Consistent with the IF results, this response was ablated in MEFs expressing R128E-, 4A2-, or 6A-3XFLAG but not in MEFs expressing the pocket mutants. Thus, genotoxin-induced 9-1-1 clamp accumulation on damaged DNA requires proper 9-1-1 clamp formation and DNA interactions but not HUS1 pocket-mediated functions.

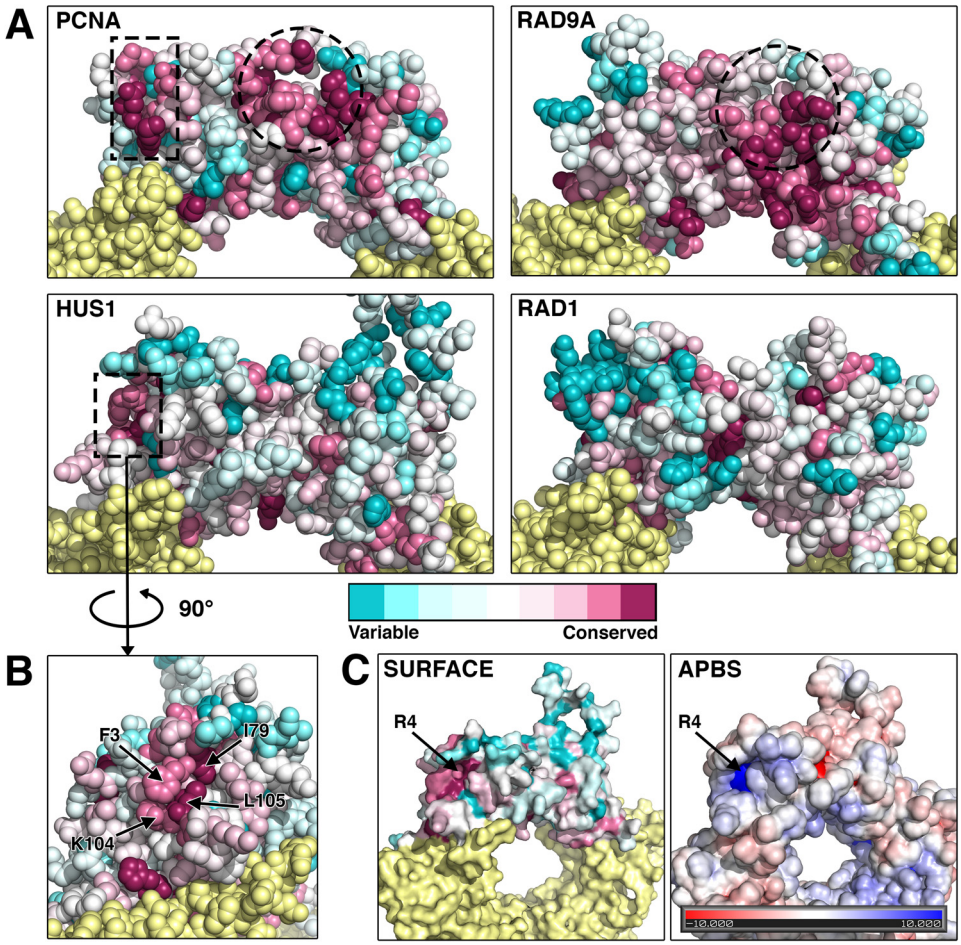

FIGURE 4. **The identification of a novel conserved hydrophobic pocket on the outer surface of HUS1.** *A* and *B*, the evolutionary conservation values of each amino acid position in the protein structures of PCNA, RAD9A, HUS1, and RAD1 were calculated using the Consurf bioinformatics server (see "Experimental Procedures"). Multiple sequence alignments of 44 organisms that encompass a wide range of taxa were used (see Table 2). Residues *pseudocolored* in *cyan* have diverged and are variable, whereas those in *magenta* are conserved. *Dotted lines* outline conserved regions that potentially mediate protein-protein associations. The *circled regions* correspond to the PIP box-binding hydrophobic pocket of PCNA and the analogous conserved region of RAD9A. A second conserved region for PCNA and HUS1 is outlined with a *rectangle* and in the case of HUS1 corresponds to a novel pocket on the side of globular domain 1 composed of 3 conserved hydrophobic residues. *C*, HUS1 atomic surface and surface electrostatic potential models reveal a positively charged groove at the base of the novel pocket. The charge is contributed by an arginine at position 4.

HUS1 Pocket Mutants Are Competent for Checkpoint Signaling but Defective for Effector Interactions—To determine whether the various mHUS1 mutants affected ATR activation and checkpoint signaling, we assessed UV-induced CHK1 phosphorylation (pCHK1) (Fig. 7*A*). As reported previously (20), *Hus1*-null MEFs were impaired for CHK1 phosphorylation upon UV treatment. This defect was rectified by complementation with WT mHUS1. However, in cells complemented with the mHUS1 R128E, 4A-2, or 6A mutants, the pCHK1 response was abrogated to the same extent as with complete *mHus1* deficiency. These data indicate that unstable subunit-subunit and mHUS1-DNA interactions significantly impair ATR activation, consistent with the observations that these mutant proteins failed to properly localize to DNA damage sites. By contrast, cells expressing mHUS1 pocket mutants I152Y, R4D, or R4D,I152Y retained normal levels of UV-induced CHK1 phosphorylation (Fig. 7*A*), as might be expected because interactions between 9-1-1 and the ATR activator TOPBP1 occur through RAD9A (17). This result suggests that the genotoxin sensitivity phenotype shown by cells expressing the pocket mutants might be due to disruption of checkpoint signaling-independent HUS1 functions.

The 9-1-1 clamp is known to interact with several DNA repair proteins, including many from the base excision repair pathway (18, 19). Among the well-established 9-1-1 binding partners is the DNA glycosylase MutY homolog (MYH) (33, 34). In order to determine whether HUS1 outer surface pockets were important for protein-protein interactions, R4D,I152Y-3XFLAG protein was expressed and immunoprecipitated for the detection of association with endogenous MYH (Fig. 7*B*). Whereas wild-type HUS1–3XFLAG effectively pulled down MYH, less MYH was detected in the R4D,I152Y-3XFLAG immunoprecipitation. Notably, TOPBP1 co-immunoprecipitated with the HUS1 outer surface mutant to a similar extent as with wild-type HUS1, consistent with our observation that this mutant was capable of promoting UV-induced CHK1 phosphorylation. Together, these results indicate that the mHUS1 outer surface mutant is defective for the recruitment of DNA repair proteins despite properly localizing to damaged DNA and supporting ATR checkpoint signaling,

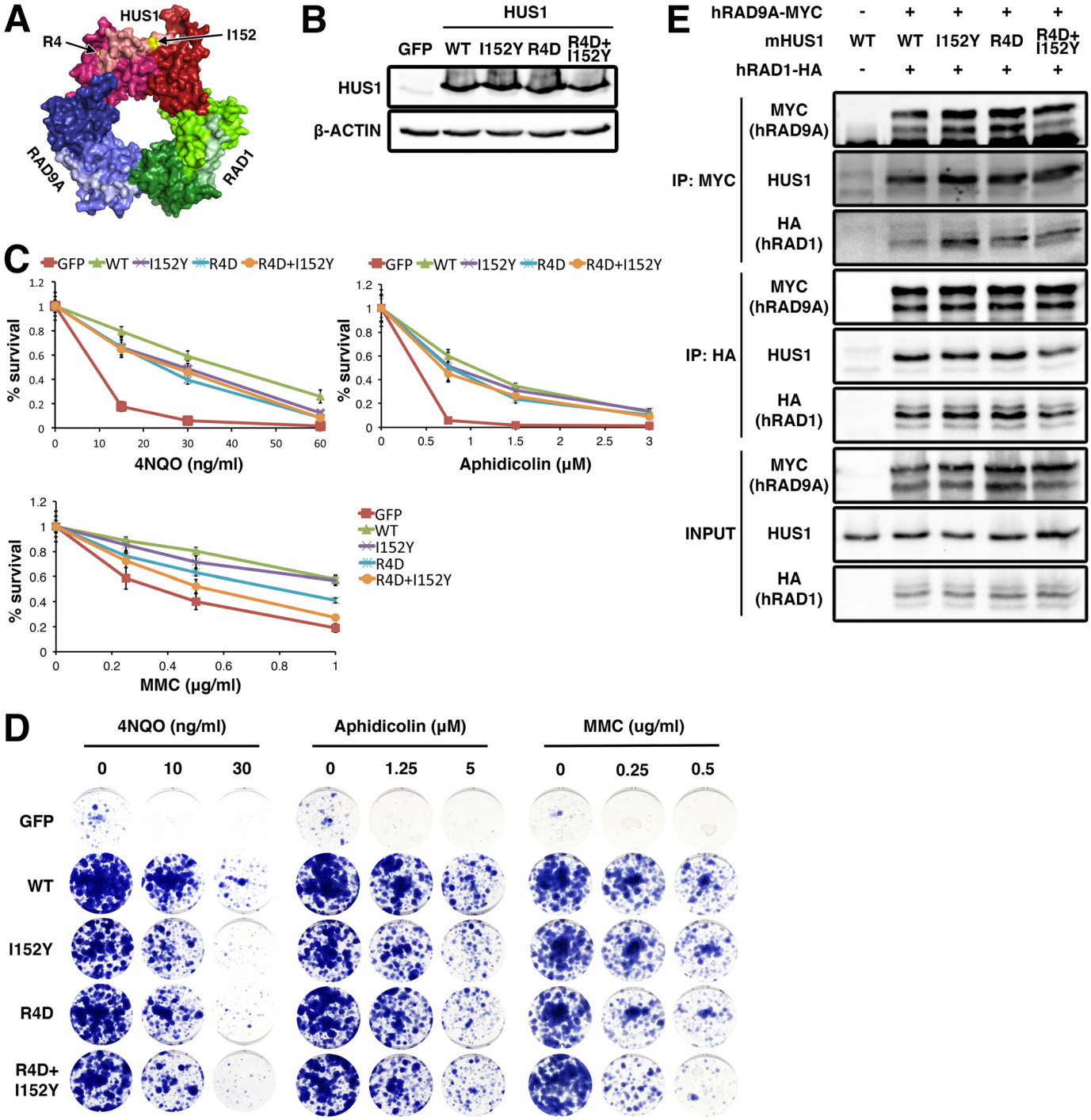

FIGURE 5. **Two hydrophobic pockets on the outer surface of HUS1 are required for genotoxic stress responses.** *A*, Arg-4 and Ile-152 (*arrows*) are located on the outer ring surface (Protein Data Bank code 3GGR). *B*, protein expression was measured as in Fig. 1*B*. *C* and *D*, genotoxin sensitivity was measured as in Fig. 1, *C* and *D*, as well as with MMC treatment. Each experiment in *C* was repeated two times with two independently generated cell lines. *E*, interaction of the pocket mutants with hRAD9 and hRAD1 was assessed by co-IP. *Error bars*, S.D.

highlighting ATR-independent effector functions downstream of HUS1 (Fig. 7*C*).

Discussion

Checkpoint signaling in coordination with appropriate DNA repair is crucial for a successful DDR in cells experiencing various genotoxic stresses. Understanding this concerted action is important for appreciating how normal cells are protected from the deleterious effects of genomic instability and how malignant cells manage genomic and cellular integrity in the face of numerous physiological stresses (35–38). In this study, we sought to understand the molecular interactions that underlie a robust DDR involving the 9-1-1 clamp and in doing so defined both the molecular requirements for stimulation of ATR-induced CHK1 phosphorylation and CHK1-independent functions for the 9-1-1 complex mediated by outer surface residues of the HUS1 subunit.

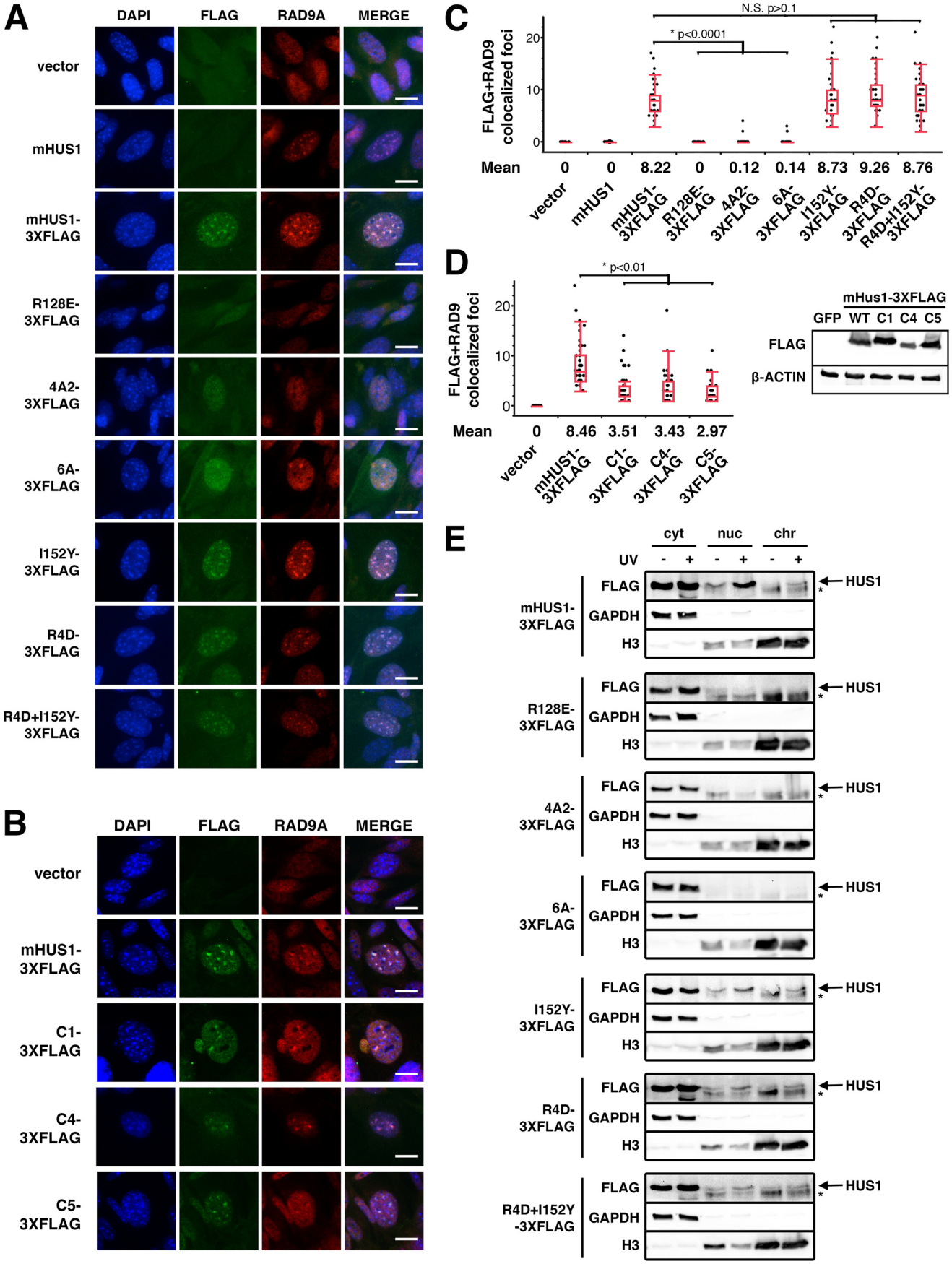
A
DAPI
FLAG
RAD9A
MERGE
vector
mHUS1
mHUS1-3XFLAG
R128E-3XFLAG
4A2-3XFLAG
6A-3XFLAG
I152Y-3XFLAG
R4D-3XFLAG
R4D+I152Y-3XFLAG
B
DAPI
FLAG
RAD9A
MERGE
vector
mHUS1-3XFLAG
C1-3XFLAG
C4-3XFLAG
C5-3XFLAG
C
FLAG+RAD9 colocalized foci
N.S. p>0.1
* p<0.0001
Mean
0
0
8.22
0
0.12
0.14
8.73
9.26
8.76
vector
mHUS1
mHUS1-3XFLAG
R128E-3XFLAG
4A2-3XFLAG
6A-3XFLAG
I152Y-3XFLAG
R4D-3XFLAG
R4D+I152Y-3XFLAG
D
FLAG+RAD9 colocalized foci
* p<0.01
Mean
0
8.46
3.51
3.43
2.97
vector
mHUS1-3XFLAG
C1-3XFLAG
C4-3XFLAG
C5-3XFLAG
mHus1-3XFLAG
GFP
WT
C1
C4
C5
FLAG
β-ACTIN
E
cyt
nuc
chr
UV
- + - + - +
mHUS1-3XFLAG
R128E-3XFLAG
4A2-3XFLAG
6A-3XFLAG
I152Y-3XFLAG
R4D-3XFLAG
R4D+I152Y-3XFLAG
FLAG
GAPDH
H3
HUS1

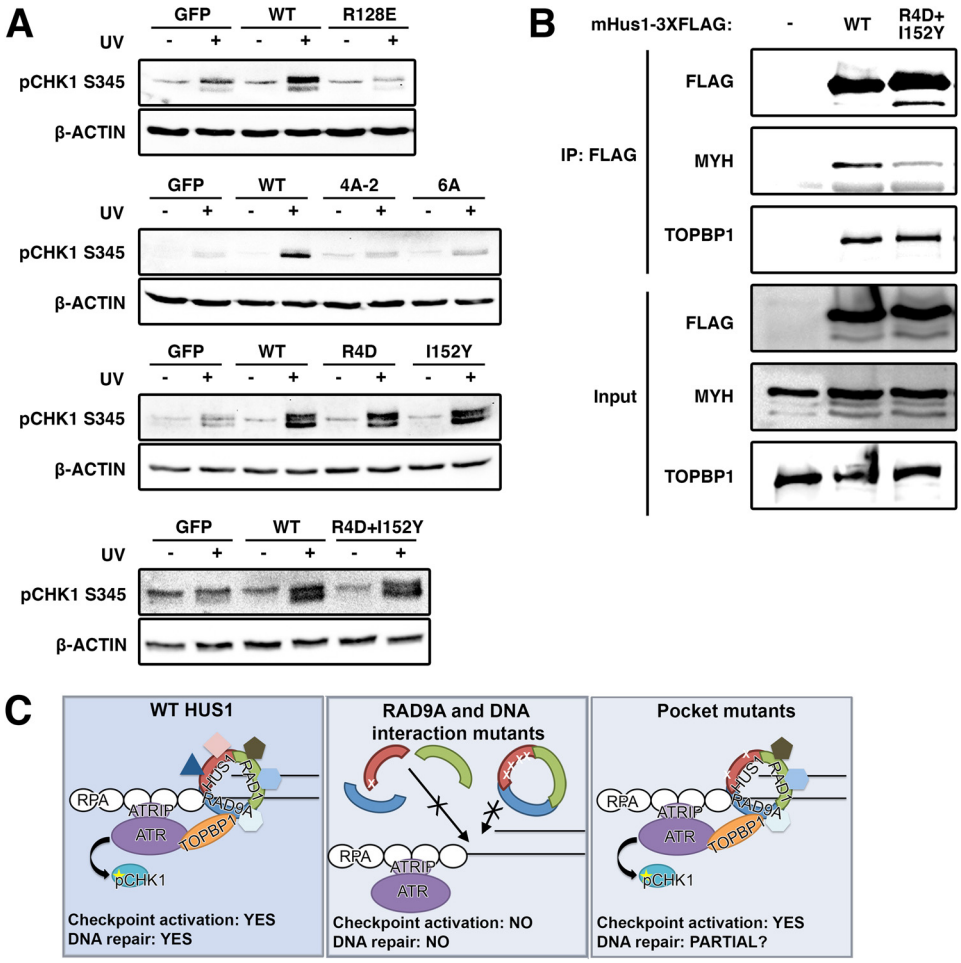

FIGURE 7. **9-1-1-dependent checkpoint signaling requires clamp formation and DNA associations but not HUS1 outer surface pocket function, which is necessary for effector interactions.** *A*, DNA damage-induced CHK1 phosphorylation is hampered in HUS1 clamp formation and DNA interaction mutants but is intact for HUS1 outer surface pocket mutants. Lysates from cells treated with 0 or 100 J/m^2 UV were immunoblotted using antibodies specific for phospho-CHK1 or β-actin. *B*, HUS1 pocket mutant R4D,I152Y is impaired for interaction with base excision repair protein MYH. Lysates prepared from HEK293T cells overexpressing 3XFLAG-tagged WT or R4D,I152Y mHUS1 proteins were immunoprecipitated with antibody specific for FLAG and immunoblotted using antibodies specific for MYH and TOPBP1. *C*, model for HUS1-mediated function in DNA damage response. WT HUS1 forms 9-1-1 clamps, localizes to DNA damage sites, and mediates ATR checkpoint signaling and DNA repair functions. When the RAD9A-interacting residue is dysfunctional, HUS1 cannot form 9-1-1 clamp, causing loss of all downstream functions. HUS1 mutants defective for DNA interactions are still able to form 9-1-1 clamps but cannot localize to DNA damage sites, similarly causing loss of all downstream functions. Only HUS1 pocket mutants are able to form 9-1-1 clamps, localize to DNA lesions, and activate ATR for checkpoint signaling. However, checkpoint-independent functions of HUS1 are perturbed in the pocket mutants, probably causing increased genotoxin hypersensitivity due to impaired DNA repair.

Maintaining sufficient intersubunit contacts is the most crucial initial step for 9-1-1 clamp formation, failure of which will abrogate all downstream clamp functions. Remarkably, reversing the polarity of a single residue (Arg-128 of mHUS1) at the RAD9A/HUS1 interface fully disrupted 9-1-1 clamp integrity and function, although there are at least 8 other HUS1 residues predicted to contribute to RAD9A-HUS1 interactions (28). Interestingly, the RAD9A/HUS1 interface mutation also disrupted HUS1-RAD1 and RAD1-RAD9A associations. One possible explanation is that active repulsion of HUS1-RAD9A indirectly weakens HUS1-RAD1 and RAD9A-RAD1 interactions. Alternatively, the findings may suggest that clamp assembly occurs in an ordered, stepwise process, as reported for the heterotrimeric PCNA of *Sulfoflobus solfataricus* (*Sso*PCNA) (39), or that all three 9-1-1 interfaces function cooperatively during trimerization.

The inner surface of PCNA consists of four parallel α-helices that contain positively charged residues, some of which contact the negatively charged DNA sugar-phosphate backbone and are necessary for efficient clamp loading and mobility on DNA (40). Similarly, the HUS1 inner surface also is composed of four parallel α-helices containing numerous positively charged residues, and here we report that HUS1 function requires a specific set of synergistically important residues that are aligned in a

FIGURE 6. **DNA damage-induced HUS1 localization is defective in HUS1 clamp-forming and DNA-interacting mutants but not in HUS1 pocket mutants.** *A* and *B*, MMC-treated *Hus1*-null MEFs stably expressing the indicated constructs were stained with DAPI (*blue*) and α-FLAG (*green*) and α-RAD9A (*red*) antibodies. *Scale bar*, 10 μm. *C* and *D*, quantifications of colocalized FLAG and RAD9A foci are presented in *quartile box* and *dot plots*. *NS*, not significant. *D*, immunoblotting using antibodies specific for FLAG or β-actin was performed to compare the stability of 3XFLAG-tagged WT and mutant mHUS1 proteins (C1, C4, and C5) in HEK293T cells. *E*, cells were UV-treated; fractionated into cytoplasmic (*cyt*), nuclear (*nuc*), and chromatin (*chr*) fractions; and immunoblotted. GAPDH and histone 3 served as fractionation controls. *Arrows*, HUS1 band; *asterisks*, nonspecific band.

transhelical manner analogous to those of PCNA. Notably, our findings are consistent with predicted HUS1-DNA contacts from computational modeling (27). It is remarkable that loss of DNA contacts for the HUS1 subunit alone leads to severe checkpoint signaling defects and hypersensitivity to genotoxins, because modeling of 9-1-1 on DNA indicates that the three subunits contribute almost equally for DNA backbone associations (27), although it remains possible that certain DNA structures might lead to other 9-1-1 conformations on DNA. The HUS1 inner surface mutants stably associate with the other 9-1-1 subunits but do not show substantial DNA damage-induced accumulation on chromatin, suggesting that interactions between 9-1-1 and DNA are necessary for stable loading of the clamp.

Much knowledge about PCNA function was gained by structure/function studies that identified a PCNA hydrophobic pocket as the docking site for most PIP box motif-carrying proteins (41). Based on the structural similarity between the 9-1-1 complex and PCNA, we hypothesized that the outer surface of HUS1 would mediate physical interactions with downstream effectors. Our evolutionary conservation analysis revealed that among all 9-1-1 subunits, RAD9A showed the greatest conservation of the hydrophobic pocket that is analogous to the site where PCNA interacts with PCNA-interacting protein box motifs, consistent with the idea that RAD9A is the subunit most closely related to PCNA (12). The same region was conserved among mammalian HUS1 proteins but not in a broader representation of species. This suggests that whereas the RAD9A pocket is evolutionarily conserved, HUS1 and RAD1 have undergone greater divergence, potentially reflecting specialization of clamp subunits. Consurf analysis of HUS1 additionally revealed a second hydrophobic pocket on the outer surface that showed substantial evolutionary conservation. Disruption of these two HUS1 outer surface pockets caused partial loss of function without disturbing clamp formation or its recruitment to chromatin following DNA damage. That cells expressing these pocket mutants were not as hypersensitive to genotoxic stress as cells that completely lack HUS1 probably relates to the fact that they remain functional for genotoxin-induced CHK1 activation, as would be expected because interactions between 9-1-1 and the ATR activator TOPBP1 occur through the C-terminal tail of RAD9A (17). It also remains possible that RAD9A and RAD1 provide some level of redundancy when HUS1 is dysfunctional, because in some cases, RAD9A, HUS1, and RAD1 can all interact with the same repair protein, albeit with different binding affinities (42–47). We favor the possibility that each 9-1-1 subunit binds at least some unique downstream effectors, with the idea that each subunit is specialized to some extent to mediate specific functions. Indeed, the subunits of the archaeal heterotrimeric PCNA each interact with distinct binding partners, a characteristic that provides a means to diversify and coordinate clamp functions (48).

PCNA-effector interactions invariably involve PIP box sequences, but there is mixed evidence regarding a role for PIP box motifs in 9-1-1-effector interactions (3), and the role of the secondary HUS1 pocket is unknown. It may stabilize interactions with PIP box-containing effectors that bind the primary pocket, resembling PCNA interactions with FEN1 and p21 (31, 32). Combining the outer surface mutations (R4D,I152Y) did not further increase hypersensitivity to 4NQO or aphidicolin beyond that for either single mutant (Table 3), suggesting a related function for the two pockets. However, cells expressing the double mutant R4D,I152Y showed increased sensitivity to MMC, consistent with our previous findings.[3] Here we further show that the double mutant R4D,I152Y confers greater MMC hypersensitivity than either of the corresponding single mutants, implying that at certain DNA lesions, the two HUS1 pockets can have separate roles that cooperatively improve cell survival. In such circumstances, the secondary HUS1 pocket might interact with distinct effectors independently of the primary pocket, through a different motif, like the recently reported Mec3-Mcm10 interaction, which involves both a PIP box and other sequences in MCM10 (49). With its close proximity to the RAD9A primary PCNA-like pocket, the secondary HUS1 pocket also may be involved in RAD9A-HUS1 intersubunit-effector binding, as has been reported for the interaction between the equivalent budding yeast proteins (DDC1-MEC3) and their partner RED1 (50). Bacterial β-clamp and *Sso*PCNA similarly display intersubunit interactions with TLS polymerases (51, 52).

An open question has been to what extent the requirement for the 9-1-1 complex in genome maintenance reflects its role in TOPBP1-induced ATR activation *versus* direct functions for 9-1-1 subunits in other processes. By mutating the HUS1 outer surface pockets, we have successfully separated these 9-1-1 functions and demonstrate that HUS1 has roles apart from checkpoint signaling that also are crucial for cell survival following DNA damage. Continued analysis of this collection of HUS1 mutants, especially further dissection of the genotoxin-specific functions of both HUS1 outer surface pockets, as well as the outer surface domains of RAD9A and RAD1, holds promise for shedding light on 9-1-1 functions in genome maintenance and highlighting potential targets that can be exploited clinically for anti-cancer therapies.

Acknowledgments—We thank Ivaylo Ivanov, Alba Guarne, Joseph Peters, and Marcus Smolka for helpful discussions and comments on the manuscript.

References

1. Jackson, S. P., and Bartek, J. (2009) The DNA-damage response in human biology and disease. *Nature* **461,** 1071–1078
2. Cimprich, K. A., and Cortez, D. (2008) ATR: an essential regulator of genome integrity. *Nat. Rev. Mol. Cell Biol.* **9,** 616–627
3. Eichinger, C. S., and Jentsch, S. (2011) 9-1-1: PCNA's specialized cousin. *Trends Biochem. Sci.* **36,** 563–568
4. Hopkins, K. M., Auerbach, W., Wang, X. Y., Hande, M. P., Hang, H., Wolgemuth, D. J., Joyner, A. L., and Lieberman, H. B. (2004) Deletion of mouse rad9 causes abnormal cellular responses to DNA damage, genomic instability, and embryonic lethality. *Mol. Cell Biol.* **24,** 7235–7248
5. Han, L., Hu, Z., Liu, Y., Wang, X., Hopkins, K. M., Lieberman, H. B., and Hang, H. (2010) Mouse Rad1 deletion enhances susceptibility for skin

[3] Balmus, G., Lim, P. X., Oswald, A., Hume, K. R., Cassano, A., Pierre, J., Hill, A., Huang, W., August, A., Stokol, T., Southard, T., and Weiss, R. S. (2015) HUS1 regulates *in vivo* responses to genotoxic chemotherapies. *Oncogene* 10.1038/onc.2015.118

tumor development. *Mol. Cancer* **9,** 67
6. Weiss, R. S., Enoch, T., and Leder, P. (2000) Inactivation of mouse Hus1 results in genomic instability and impaired responses to genotoxic stress. *Genes Dev.* **14,** 1886–1898
7. Yazinski, S. A., Westcott, P. M., Ong, K., Pinkas, J., Peters, R. M., and Weiss, R. S. (2009) Dual inactivation of Hus1 and p53 in the mouse mammary gland results in accumulation of damaged cells and impaired tissue regeneration. *Proc. Natl. Acad. Sci. U.S.A.* **106,** 21282–21287
8. Lyndaker, A. M., Lim, P. X., Mleczko, J. M., Diggins, C. E., Holloway, J. K., Holmes, R. J., Kan, R., Schlafer, D. H., Freire, R., Cohen, P. E., and Weiss, R. S. (2013) Conditional inactivation of the DNA damage response gene Hus1 in mouse testis reveals separable roles for components of the RAD9-RAD1-HUS1 complex in meiotic chromosome maintenance. *PLoS Genet.* **9,** e1003320
9. Vasileva, A., Hopkins, K. M., Wang, X., Weisbach, M. M., Friedman, R. A., Wolgemuth, D. J., and Lieberman, H. B. (2013) The DNA damage checkpoint protein RAD9A is essential for male meiosis in the mouse. *J. Cell Sci.* **126,** 3927–3938
10. Moldovan, G. L., Pfander, B., and Jentsch, S. (2007) PCNA, the maestro of the replication fork. *Cell* **129,** 665–679
11. Xu, M., Bai, L., Gong, Y., Xie, W., Hang, H., and Jiang, T. (2009) Structure and functional implications of the human rad9-hus1-rad1 cell cycle checkpoint complex. *J. Biol. Chem.* **284,** 20457–20461
12. Doré, A. S., Kilkenny, M. L., Rzechorzek, N. J., and Pearl, L. H. (2009) Crystal structure of the rad9-rad1-hus1 DNA damage checkpoint complex: implications for clamp loading and regulation. *Mol. Cell* **34,** 735–745
13. Sohn, S. Y., and Cho, Y. (2009) Crystal structure of the human rad9-hus1-rad1 clamp. *J. Mol. Biol.* **390,** 490–502
14. Ellison, V., and Stillman, B. (2003) Biochemical characterization of DNA damage checkpoint complexes: clamp loader and clamp complexes with specificity for 5′ recessed DNA. *PLoS Biol.* **1,** E33
15. Bermudez, V. P., Lindsey-Boltz, L. A., Cesare, A. J., Maniwa, Y., Griffith, J. D., Hurwitz, J., and Sancar, A. (2003) Loading of the human 9-1-1 checkpoint complex onto DNA by the checkpoint clamp loader hRad17-replication factor C complex *in vitro*. *Proc. Natl. Acad. Sci. U.S.A.* **100,** 1633–1638
16. Majka, J., Binz, S. K., Wold, M. S., and Burgers, P. M. (2006) Replication protein A directs loading of the DNA damage checkpoint clamp to 5′-DNA junctions. *J. Biol. Chem.* **281,** 27855–27861
17. Delacroix, S., Wagner, J. M., Kobayashi, M., Yamamoto, K., and Karnitz, L. M. (2007) The Rad9-Hus1-Rad1 (9-1-1) clamp activates checkpoint signaling via TopBP1. *Genes Dev.* **21,** 1472–1477
18. Helt, C. E., Wang, W., Keng, P. C., and Bambara, R. A. (2005) Evidence that DNA damage detection machinery participates in DNA repair. *Cell Cycle* **4,** 529–532
19. Madabushi, A., and Lu, A.-L. (2011) The novel role of cell cycle checkpoint clamp Rad9-Hus1-Rad1 (the 9-1-1 complex) in DNA repair. in *Advances in Medicine and Biology* (Berhardt, L. V., ed) pp. 41–74, Nova Science Publishers, Hauppauge, NY
20. Weiss, R. S., Matsuoka, S., Elledge, S. J., and Leder, P. (2002) Hus1 acts upstream of Chk1 in a mammalian DNA damage response pathway. *Curr. Biol.* **12,** 73–77
21. Hinds, P. W., Finlay, C. A., Quartin, R. S., Baker, S. J., Fearon, E. R., Vogelstein, B., and Levine, A. J. (1990) Mutant p53 DNA clones from human colon carcinomas cooperate with ras in transforming primary rat cells: a comparison of the "hot spot" mutant phenotypes. *Cell Growth Differ.* **1,** 571–580
22. Thompson, J. D., Gibson, T. J., Plewniak, F., Jeanmougin, F., and Higgins, D. G. (1997) The CLUSTAL_X Windows interface: flexible strategies for multiple sequence alignment aided by quality analysis tools. *Nucleic Acids Res.* **25,** 4876–4882
23. Ashkenazy, H., Erez, E., Martz, E., Pupko, T., and Ben-Tal, N. (2010) ConSurf 2010: calculating evolutionary conservation in sequence and structure of proteins and nucleic acids. *Nucleic Acids Res.* **38,** W529–W533
24. Gu, Y., and Lu, A.-L. (2001) Differential DNA recognition and glycosylase activity of the native human MutY hmolog (hMYH) and recombinant hMYH expressed in bacteria. *Nucleic Acids Res.* **29,** 2666–2674
25. Rendtlew Danielsen, J. M., Larsen, D. H., Schou, K. B., Freire, R., Falck, J., Bartek, J., and Lukas, J. (2009) HCLK2 is required for activity of the DNA damage response kinase ATR. *J. Biol. Chem.* **284,** 4140–4147
26. Abmayr, S. M., Yao, T., Parmely, T., and Workman, J. L. (2001) Preparation of nuclear and cytoplasmic extracts from mammalian cells. *Curr. Protoc. Mol. Biol.* 10.1002/0471142727.mb1201s75
27. Querol-Audí, J., Yan, C., Xu, X., Tetsukawa, S. E., Tsai, M.-S., Tainer, J. A., Cooper, P. K., Nogales, E., and Ivanov, I. (2012) Repair complexes of FEN1 endonuclease, DNA, and Rad9-Hus1-Rad1 are distinguished from their PCNA counterparts by functionally important stability. *Proc. Natl. Acad. Sci. U.S.A.* **109,** 8528–8533
28. Xu, X., Guardiani, C., Yan, C., and Ivanov, I. (2013) Opening pathways of the DNA clamps proliferating cell nuclear antigen and Rad9-Rad1-Hus1. *Nucleic Acids Res.* **41,** 10020–10031
29. Kaur, R., Kostrub, C. F., and Enoch, T. (2001) Structure-function analysis of fission yeast Hus1-Rad1-Rad9 checkpoint complex. *Mol. Biol. Cell* **12,** 3744–3758
30. McNally, R., Bowman, G. D., Goedken, E. R., O'Donnell, M., and Kuriyan, J. (2010) Analysis of the role of PCNA-DNA contacts during clamp loading. *BMC Struct. Biol.* **10,** 3
31. Gulbis, J. M., Kelman, Z., Hurwitz, J., O'Donnell, M., and Kuriyan, J. (1996) Structure of the C-terminal region of p21WAF1/CIP1 complexed with human PCNA. *Cell* **87,** 297–306
32. Sakurai, S., Kitano, K., Yamaguchi, H., Hamada, K., Okada, K., Fukuda, K., Uchida, M., Ohtsuka, E., Morioka, H., and Hakoshima, T. (2005) Structural basis for recruitment of human flap endonuclease 1 to PCNA. *EMBO J.* **24,** 683–693
33. Chang, D. Y., and Lu, A. L. (2005) Interaction of checkpoint proteins Hus1/Rad1/Rad9 with DNA base excision repair enzyme MutY homolog in fission yeast, *Schizosaccharomyces pombe*. *J. Biol. Chem.* **280,** 408–417
34. Shi, G., Chang, D. Y., Cheng, C. C., Guan, X., Venclovas, C., and Lu, A. L. (2006) Physical and functional interactions between MutY glycosylase homologue (MYH) and checkpoint proteins Rad9-Rad1-Hus1. *Biochem. J.* **400,** 53–62
35. Helleday, T., Petermann, E., Lundin, C., Hodgson, B., and Sharma, R. A. (2008) DNA repair pathways as targets for cancer therapy. *Nat. Rev. Cancer* **8,** 193–204
36. Hoeijmakers, J. (2001) Genome maintenance mechanisms for preventing cancer. *Nature* **411,** 366–374
37. Ciccia, A., and Elledge, S. J. (2010) The DNA damage response: making it safe to play with knives. *Mol. Cell* **40,** 179–204
38. Hanahan, D., and Weinberg, R. A. (2011) Hallmarks of cancer: the next generation. *Cell* **144,** 646–674
39. Dionne, I., Nookala, R. K., Jackson, S. P., Doherty, A. J., and Bell, S. D. (2003) A heterotrimeric PCNA in the hyperthermophilic achaeon *Sulfolobus solfatoricus*. *Mol. Cell* **11,** 275–282
40. Georgescu, R. E., Kim, S. S., Yurieva, O., Kuriyan, J., Kong, X. P., and O'Donnell, M. (2008) Structure of a sliding clamp on DNA. *Cell* **132,** 43–54
41. Naryzhny, S. N. (2008) Proliferating cell nuclear antigen: a proteomics view. *Cell Mol. Life Sci.* **65,** 3789–3808
42. Friedrich-Heineken, E., Toueille, M., Tännler, B., Bürki, C., Ferrari, E., Hottiger, M. O., and Hübscher, U. (2005) The two DNA clamps Rad9/Rad1/Hus1 complex and proliferating cell nuclear antigen differentially regulate flap endonuclease 1 activity. *J. Mol. Biol.* **353,** 980–989
43. Smirnova, E., Toueille, M., Markkanen, E., and Hübscher, U. (2005) The human checkpoint sensor and alternative DNA clamp Rad9-Rad1-Hus1 modulates the activity of DNA ligase I, a component of the long-patch base excision repair machinery. *Biochem. J.* **389,** 13–17
44. Gembka, A., Toueille, M., Smirnova, E., Poltz, R., Ferrari, E., Villani, G., and Hübscher, U. (2007) The checkpoint clamp, Rad9-Rad1-Hus1 complex, preferentially stimulates the activity of apurinic/apyrimidinic endonuclease 1 and DNA polymerase β in long patch base excision repair. *Nucleic Acids Res.* **35,** 2596–2608
45. Guan, X., Madabushi, A., Chang, D. Y., Fitzgerald, M. E., Shi, G., Drohat, A. C., and Lu, A. L. (2007) The human checkpoint sensor Rad9-Rad1-

Hus1 interacts with and stimulates DNA repair enzyme TDG glycosylase. *Nucleic Acids Res.* **35,** 6207–6218

46. Park, M. J., Park, J. H., Hahm, S. H., Ko, S. I., Lee, Y. R., Chung, J. H., Sohn, S. Y., Cho, Y., Kang, L. W., and Han, Y. S. (2009) Repair activities of human 8-oxoguanine DNA glycosylase are stimulated by the interaction with human checkpoint sensor Rad9-Rad1-Hus1 complex. *DNA Repair* **8,** 1190–1200
47. Bai, H., Madabushi, A., Guan, X., and Lu, A. L. (2010) Interaction between human mismatch repair recognition proteins and checkpoint sensor Rad9-Rad1-Hus1. *DNA Repair* **9,** 478–487
48. Beattie, T. R., and Bell, S. D. (2012) Coordination of multiple enzyme activities by a single PCNA in archaeal Okazaki fragment maturation. *EMBO J.* **31,** 1556–1567
49. Alver, R. C., Zhang, T., Josephrajan, A., Fultz, B. L., Hendrix, C. J., Das-Bradoo, S., and Bielinsky, A. K. (2014) The N-terminus of Mcm10 is important for interaction with the 9-1-1 clamp and in resistance to DNA damage. *Nucleic Acids Res.* **42,** 8389–8404
50. Eichinger, C. S., and Jentsch, S. (2010) Synaptonemal complex formation and meiotic checkpoint signaling are linked to the lateral element protein Red1. *Proc. Natl. Acad. Sci. U.S.A.* **107,** 11370–11375
51. Bunting, K. A., Roe, S. M., and Pearl, L. H. (2003) Structural basis for recruitment of transletion DNA polymerase Pol IV/DinB to the β-clamp. *EMBO J.* **22,** 5883–5892
52. Xing, G., Kirouac, K., Shin, Y. J., Bell, S. D., and Ling, H. (2009) Structural insight into recruitment of translesion DNA polymerase Dpo4 to sliding clamp PCNA. *Mol. Microbiol.* **71,** 678–691